European Journal of Pharmacology 884 (2020) 173303

Contents lists available at ScienceDirect

European Journal of Pharmacology

journal homepage: www.elsevier.com/locate/ejphar

Full length article

Propofol induces the elevation of intracellular calcium via morphological changes in intracellular organelles, including the endoplasmic reticulum and mitochondria

Tomoaki Urabe [a,b], Yuhki Yanase [c], Serika Motoike [d], Kana Harada [a], Izumi Hide [a], Shigeru Tanaka [a], Yasuo M. Tsutsumi [b], Masashi Kawamoto [b,e], Norio Sakai [a,*]

[a] Department of Molecular and Pharmacological Neuroscience, Graduate School of Biomedical & Health Sciences, Hiroshima University, 1-2-3 Kasumi, Minami-ku, Hiroshima, 734-8551, Japan
[b] Department of Anesthesiology and Critical Care, Graduate School of Biomedical & Health Sciences, Hiroshima University, 1-2-3 Kasumi, Minami-ku, Hiroshima, 734-8551, Japan
[c] Department of Dermatology, Graduate School of Biomedical & Health Sciences, Hiroshima University, 1-2-3 Kasumi, Minami-ku, Hiroshima, 734-8551, Japan
[d] Department of Dental Anesthesiology, Graduate School of Biomedical & Health Sciences, Hiroshima University, 1-2-3 Kasumi, Minami-ku, Hiroshima, 734-8551, Japan
[e] Medical Corporation JR Hiroshima Hospital, 3-1-36 Futabanosato, Higashi-Ku, Hiroshima, 732-0057, Japan

ARTICLE INFO

Keywords:
Propofol
Intracellular calcium
Endoplasmic reticulum (ER)
Mitochondria
Angialgia

ABSTRACT

Propofol, most frequently used as a general anesthetic due to its versatility and short-acting characteristics, is thought to exert its anesthetic actions via $GABA_A$ receptors; however, the precise mechanisms of its adverse action including angialgia remain unclear. We examined the propofol-induced elevation of intracellular calcium and morphological changes in intracellular organelles using SHSY-5Y neuroblastoma cells, COS-7 cells, HEK293 cells, and HUVECs loaded with fluorescent dyes for live imaging. Although propofol (>50 μM) increased intracellular calcium in a dose-dependent manner in these cells, it was not influenced by the elimination of extracellular calcium. The calcium elevation was abolished when intracellular or intraendoplasmic reticulum (ER) calcium was depleted by BAPTA-AM or thapsigargin, respectively, suggesting that calcium was mobilized from the ER. Studies using U-73122, xestospongin C, and dantrolene revealed that propofol-induced calcium elevation was not mediated by G-protein coupled receptors, IP3 receptors, or ryanodine receptors. We performed live imaging of the ER, mitochondria and Golgi apparatus during propofol stimulation using fluorescent dyes. Concomitant with the calcium elevation, the structure of the ER and mitochondria was fragmented and aggregated, and these changes were not reversed during the observation period, suggesting that propofol-induced calcium elevation occurs due to calcium leakage from these organelles. Although the concentration of propofol used in this experiment was greater than that used clinically (30 μM), it is possible that the concentration exceeds 30 μM at the site where propofol is injected, leading the idea that these phenomena might relate to the various propofol-induced adverse effects including angialgia.

1. Introduction

Propofol is used not only for the induction and maintenance of general anesthesia but also for sedating individuals receiving mechanical ventilation in the intensive care unit. Propofol is considered to be more effective than other intravenous sedatives (Cox et al., 2008). Among the several mechanisms of action of propofol, the most recognized mechanism is the direct activation of γ-aminobutyric acid A ($GABA_A$) receptors, which slows the channel closing time (Alkire et al., 2008; Franks, 2006; Irifune et al., 2003). Previous reports have also demonstrated that propofol possibly inhibits the N-methyl-D-aspartate (NMDA) receptor and modulates calcium influx through slow calcium ion channels (Kotani et al., 2008).

Although propofol is a versatile intravenous sedative agent, there are many side effects of propofol in practice. One of the most common side effects is angialgia, or pain on injection, particularly in smaller veins.

* Corresponding author.
E-mail address: nsakai@hiroshima-u.ac.jp (N. Sakai).

https://doi.org/10.1016/j.ejphar.2020.173303
Received 5 March 2020; Received in revised form 20 May 2020; Accepted 19 June 2020
Available online 15 July 2020

Other side effects include dose-dependent low blood pressure related to vasodilation and cardiorespiratory depression. A well-known serious adverse effect of propofol is propofol infusion syndrome (PRIS) (Hemphill et al., 2019). At present, PRIS is regarded as a lethal condition caused by impaired mitochondrial functions. PRIS has been reported more commonly in children and in critically ill patients after prolonged infusion of high doses of substances in combination with catecholamines and/or corticosteroids (Vasile et al., 2003).

It is controversial whether propofol has a cytoprotective or cytotoxic action in addition to the abovementioned actions. Propofol has been reported to act as a cytoprotective agent by inhibiting apoptosis mediated by ER stress and mitochondrial damage (Liu et al., 2017; Nakajima et al., 2014; Zhou et al., 2016). It has also been reported that propofol is neuroprotective in the nervous system through a variety of signaling pathways and mechanisms (Kotani et al., 2008; Li et al., 2018; Sun et al., 2018; Velly et al., 2003). In contrast, propofol has been reported to promote neuronal cell death by generating reactive oxygen species in the nervous system as a cytotoxic agent. In addition, repeated exposure to propofol reduces the expression of calcium/calmodulin-dependent kinase Iiα (CaMKIIα) and pCaMKIIα, resulting in impaired learning and memory (Gao et al., 2014). However, the precise mechanisms of these actions of propofol remain unclear.

In this study, we focused on intracellular calcium as a key to understanding the various effects of propofol. It has been reported that a high dose of propofol elevates intracellular calcium through various mechanisms (Liang et al., 2012). These reports indicate that propofol-induced calcium elevation involves intracellular mobilization of calcium via inositol 1,4,5-triphosphate (IP_3) and ryanodine receptors (RyRs) and extracellular influx via voltage-gated calcium and transient receptor potential (TRP) channels (Lawton et al., 2012; Liu et al., 2019; Nishimoto et al., 2015), but the detailed mechanisms are not fully understood. In addition, our previous study revealed that propofol at high concentrations translocates and activates calcium-dependent protein kinase C (PKC) subtypes (Miyahara et al., 2018). Since elevated intracellular calcium can drive a variety of intracellular signaling systems, we examined the propofol-induced elevation of intracellular calcium using various types of cells to identify the underlying mechanism.

2. Materials and methods

2.1. Materials

Propofol, caffeine, dantrolene, a DYKDDDDK monoclonal antibody and thapsigargin were obtained from FUJIFILM Wako Pure Chemical Industries, Ltd. (Osaka, Japan). Acetylcholine, 4',6-diamidino-2-phenylindole (DAPI) and 2,4-diisopropylphenol were purchased from Sigma-Aldrich (St. Louis, MO, USA). U-73122 and xestospongin C were purchased from Cayman Chemical Company (Ann Arbor, USA). A SEC61B polyclonal antibody was purchased from Proteintech Group Inc. (Rosemont, USA). ER-Tracker™, Fluo-4, Mito Tracker™ ResCMXRos, Alexa Flour 488-conjugated anti-rabbit IgG conjugated and Alexa Fluor 546-conjugated anti-mouse IgG were purchased from Molecular Probe (Eugene, OR, USA). CellLight ™ Golgi-GFP, BacMam2.0 and NucRed® Live 647 ReadyProbes® Reagent were purchased from Thermo Fisher Scientific (Waltham, USA).

Glass-bottom culture dishes were purchased from MatTek Corporation (Ashland, OR, USA). All of the other chemicals used were of analytical grade.

2.2. Cell culture

SHSY-5Y cells, COS-7 cells, and HEK293 cells were purchased from Riken Cell Bank (Tsukuba, Japan). Human umbilical vein endothelial cells (HUVECs) were purchased from Sumitomo Dainippon Pharma Co., Ltd. (Osaka, Japan). SHSY-5Y cells were maintained in Dulbecco's modified Eagle's medium/Ham's F-12 medium (FUJIFILM Wako, Osaka, Japan). COS-7 cells and HEK293 cells were cultured in Dulbecco's modified Eagle's medium (FUJIFILM Wako, Osaka, Japan). The medium for SHSY-5Y and COS-7 cells contained 10% bovine serum, penicillin (100 units/ml) and streptomycin (100 μg/ml). HUVECs were cultured in EBM-2 medium (CAMBREX, East Rutherford, USA) containing Clonetics EGM-2 BulletKit (CAMBREX). Culturing was performed in a humidified atmosphere containing 5% CO_2 at 37 °C in the dark. To obtain fluorescence images, cultured cells were seeded in glass-bottom culture dishes.

2.3. Loading of Fluo-4, ER-Tracker™ RED and Mito Tracker™ ResCMXRos

The cell culture medium was replaced with normal HEPES buffer composed of 165 mM NaCl, 5 mM KCl, 1 mM $MgCl_2$, 1 mM $CaCl_2$, 5 mM HEPES, and 10 mM glucose, pH 7.4. For eliminating extracellular calcium, 1 mM $CaCl_2$ was replaced with 2.5 mM EGTA. Then, cells were loaded with the calcium indicator Fluo-4 (125 μg/ml), ER-Tracker™ RED (1 μM) and Mito Tracker™ ResCMXRos (250 nM) away from light at 37 °C for 15–20 min prior to the observation of various types of cells. Pluronic 127 was also loaded for experiments using COS-7 cells and HUVECs. The concentration of Pluronic 127 did not exceed 0.025%.

2.4. Propofol treatment

Propofol was diluted with dimethyl sulfoxide (DMSO) to prepare a stock solution (100 mM). DMSO (0.1%), which almost corresponds to the concentration of DMSO when 100 μM porpofol is administered, was used as a control (0 μM propofol). Propofol was diluted to the desired concentration with normal HEPES buffer and applied to the cells to obtain the appropriate final concentration. Due to the high lipid solubility of propofol at room temperature, sonication was applied to propofol/DMSO-diluted solution immediately before the addition of propofol. The treatment concentrations and durations are described in each figure and each caption. The concentration of DMSO did not exceed 0.19%.

2.5. Observation of intracellular calcium elevation and morphological changes in intracellular organelles

Fluorescence images were obtained by fluorescence microscopy (KETENCE, BZ-9000, Osaka, Japan) or confocal microscopy (ZEISS, LSM510, Oberkochen, Germany) under appropriate excitation and emission wavelengths to detect fluorescence signals. To observe propofol-triggered calcium elevation and the morphological changes in intracellular organelles, time-lapse imaging was carried out using a fluorescence microscope after the application of propofol. In addition, to observe the details of morphological changes in intracellular organelles, such as the ER, mitochondria and the Golgi apparatus, confocal microscopy was performed.

2.6. Semiquantitative evaluation of propofol-induced intracellular calcium elevation

The time course of typical propofol-induced intracellular calcium elevation is shown in Fig. 1A. In Fig. 1B, the red and blue lines indicate the average fluorescence changes in cells in the total area and background, respectively. The differences between both lines before propofol application (b) and at the peak of calcium elevation (a) were measured. The ratio of a to b (a/b) was considered the index of propofol-induced calcium elevation.

To confirm the validity of this index, we also conducted the same experiment where the number of cells was 10 or less; thus, this index was not influenced by the number of cells in the observed area (Supplemental Fig. 1).

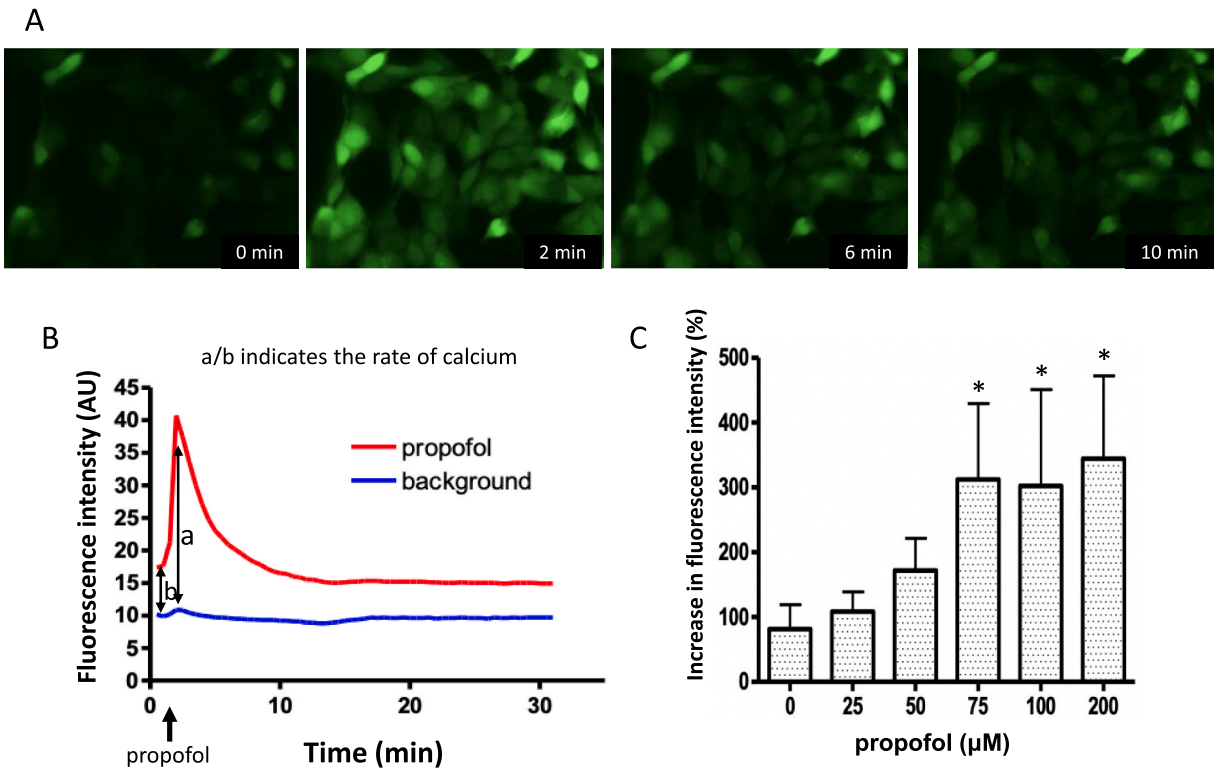

Fig. 1. Propofol-induced intracellular calcium elevation.
(A) The time course of typical propofol-induced intracellular calcium elevation is shown. Approximately two min after the application of 100 μM propofol, an increase in the fluorescence intensity of Fluo-4 was observed, indicating that intracellular calcium was increased. (B) The method used to semiquantify the rate of calcium elevation. The red line indicates the average fluorescence change over the entire observed region. The blue line indicates the fluorescence change of the background region without cells. The differences between both lines before propofol application (b) and at the peak of calcium elevation (a) were measured. The ratio of a to b (a/b) was considered an index of propofol-induced calcium elevation. (C) Propofol-induced intracellular calcium elevation was observed at concentrations between 0 and 200 μM in SHSY-5Y cells. Propofol at concentrations greater than 50 μM significantly induced the elevation of intracellular calcium in a dose-dependent manner. Data represent the mean ± SD (N = 5–21, *P < 0.05, compared to control, one-way ANOVA followed by Dunnett's posttest).

2.7. Immunocytochemistry

For the observation of ER structure, an anti-SEC61B rabbit polyclonal primary antibody (diluted 1:100) and an Alexa Flour 488-conjugated anti-rabbit IgG secondary antibody (diluted 1:500) were used. To observe the precise structure of the ER, immunocytochemistry was performed for COS-7 cells expressing FLAG-SERTΔCT, a C-terminus deleted mutant of SERT (Nobukuni et al., 2009). An expression plasmid encoding FLAG-SERTΔCT was transfected into COS-7 cells by electroporation (NEPA21, Nepagene, Japan). For immunostaining of FLAG-SERT, an anti-DYKDDDDK tag mouse monoclonal primary antibody (diluted 1:1000) and an Alexa Fluor 488-conjugated anti-mouse IgG secondary antibody (diluted 1:500) were used. Fluorescence signals were observed by confocal microscopy.

2.8. Live imaging of the Golgi apparatus

For live imaging of the Golgi apparatus, CellLight® Golgi-GFP, BacMam 2.0 (Molecular Probe) was used according to the manufacturer's recommended protocol. Fluorescence signals were observed by confocal microscopy.

2.9. Statistical analysis

We used Prism 4 software (GraphPad Software, San Diego, CA) for statistical analysis. Statistical significance was determined by one-way ANOVA followed by Dunnett's posttest or unpaired *t*-test. The difference was considered significant when the P value was less than 0.05 ($P < 0.05$).

3. Results

3.1. Characterization of propofol-induced calcium elevation

We observed a dose-dependent propofol-induced elevation of intracellular calcium at concentrations between 0 and 200 μM in SHSY-5Y cells (Fig. 1C). Propofol at a concentration greater than 50 μM significantly induced the elevation of intracellular calcium in a dose-dependent manner (see Video, Supplemental Digital Content 1, which demonstrates the 100 μM propofol-induced elevation of intracellular calcium in SHSY-5Y cells). In addition, this phenomenon was also observed in COS-7 cells, HEK293 cells, and HUVECs (Supplemental Fig. 3).

Supplementary video related to this article can be found at https://doi.org/10.1016/j.ejphar.2020.173303

3.2. Propofol-induced calcium elevation in the absence of extracellular calcium

To elucidate whether the elevation of intracellular calcium was mediated by calcium influx from the extracellular buffer, we eliminated calcium in the extracellular buffer and observed a propofol-induced elevation of intracellular calcium at concentrations between 0 and 200 μM in SHSY-5Y cells. The results showed that the propofol-induced elevation of intracellular calcium was not influenced by the elimination of extracellular calcium (Fig. 2A).

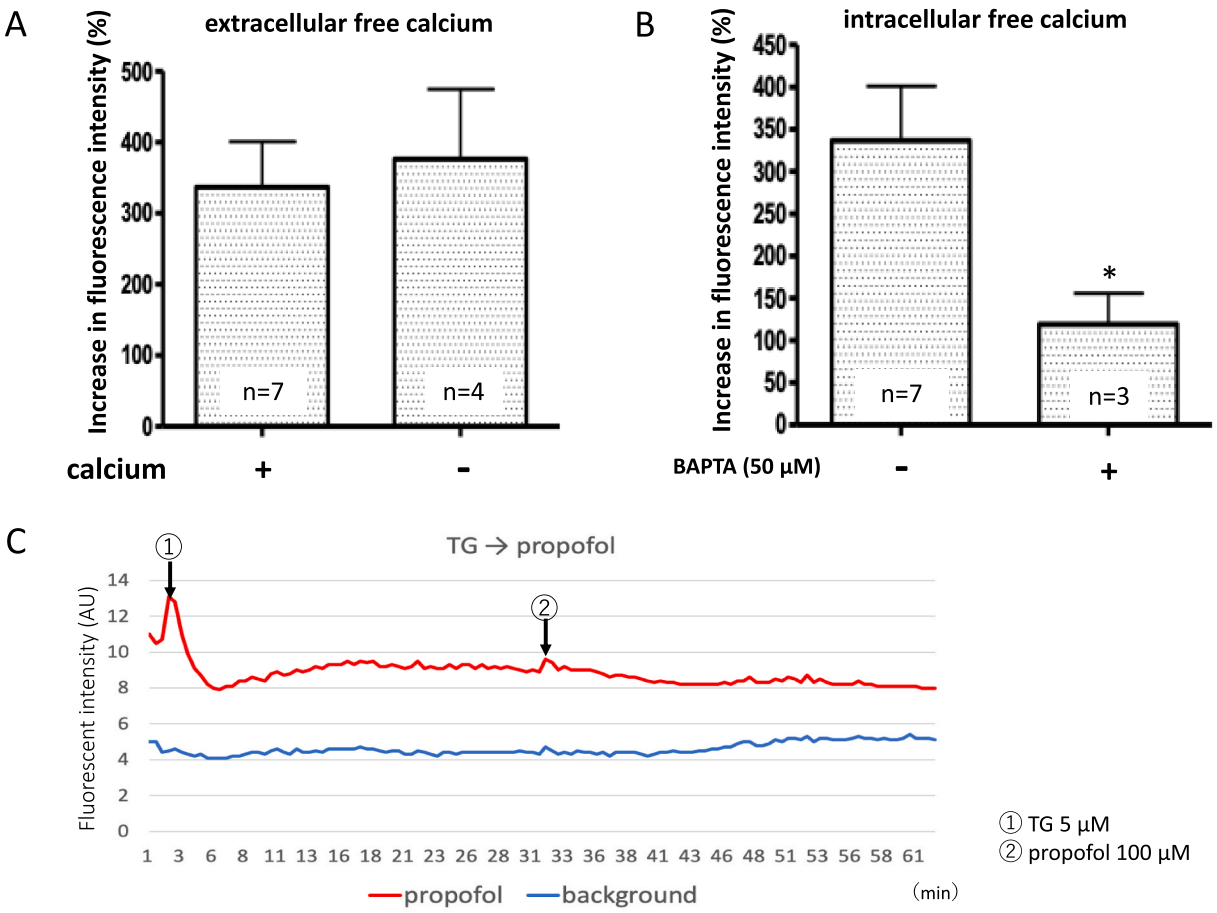

Fig. 2. Characterization of propofol-induced calcium elevation: The relationship between extracellular and intracellular calcium ions.
(A) After eliminating calcium from the extracellular buffer, a propofol-induced elevation of intracellular calcium was observed at concentrations between 0 and 200 μM in SHSY-5Y cells. The representative data indicate that the propofol (100 μM)-induced elevation of intracellular calcium was not influenced by the elimination of extracellular calcium. Data represent the mean ± SD (N = 4–7, P > 0.05, compared to control, unpaired *t*-test). No significant change was observed at other concentrations of propofol. (B) BAPTA-AM (50 μM), a calcium chelator, almost abolished the propofol (100 μM)-induced calcium elevation in SHSY-5Y cells. Data represent the mean ± SD (N = 3–7, *P < 0.01, compared to control, unpaired *t*-test). (C) Following the administration of 5 μM thapsigargin (TG), a Ca^{2+}-ATPase inhibitor (①), the [Ca^{2+}] was elevated. Subsequently, 100 μM propofol was administered 30 min after TG administration (②). Propofol did not induce any calcium elevation, suggesting that propofol mobilized calcium from the ER. Representative data out of 6 experiments is shown.

3.3. Propofol-induced calcium elevation in the absence of intracellular calcium

To elucidate the influence of intracellular calcium on propofol-induced calcium elevation, we treated the cells with BAPTA-AM (50 μM), a calcium chelator that is useful for manipulating the intracellular free calcium levels. BAPTA-AM almost abolished the propofol (100 μM)-induced calcium elevation in SHSY-5Y cells. Similar effects of BAPTA-AM were observed even with 200 μM propofol (Fig. 2B).

3.4. Effects of thapsigargin on propofol-induced calcium elevation

To elucidate whether propofol-induced calcium elevation was mobilized from the ER, we investigated the effect of thapsigargin (TG), a Ca^{2+}-ATPase inhibitor that eliminates calcium from the ER. As shown in Fig. 2C, after 5 μM TG was administered (①), the [Ca^{2+}] was elevated. Propofol was administered at a concentration of 100 μM 30 min after the TG administration, when the [Ca^{2+}] had almost returned to the basal level (②). Propofol did not induce any calcium elevation, suggesting that propofol mobilized calcium from the ER.

3.5. Mechanism underlying propofol-induced mobilization of calcium from the ER

3.5.1. Possible involvement of GPCRs in propofol-induced calcium elevation

Next, we investigated the mechanisms underlying propofol-induced intracellular calcium elevation. To elucidate the possible involvement of G-protein coupled receptors (GPCRs) in propofol-induced calcium elevation, we examined the effects of U-73122, a phospholipase C (PLC) inhibitor, on propofol-induced calcium elevation. U-73122 at 5 μM significantly inhibited the 10 μM acetylcholine-induced calcium elevation through muscarinic receptors expressed in SHSY-5Y cells. In contrast, U-73122 did not significantly affect propofol-induced calcium elevation (Fig. 3A). These results suggest that the elevation of intracellular calcium by propofol might not be mediated by GPCRs coupled with PLC.

3.5.2. Possible involvement of IP_3 and ryanodine receptors in propofol-induced calcium elevation

Calcium mobilization from ER is mediated by inositol 1,4,5-triphosphate (IP_3) or ryanodine receptors (RyRs). Therefore, we examined the effects of xestospongin C (Xc), an IP_3 receptor (IP_3R) antagonist, on propofol-induced calcium elevation. Xc at 5 μM significantly inhibited the 10 μM acetylcholine-induced calcium elevation. In contrast, Xc at 5

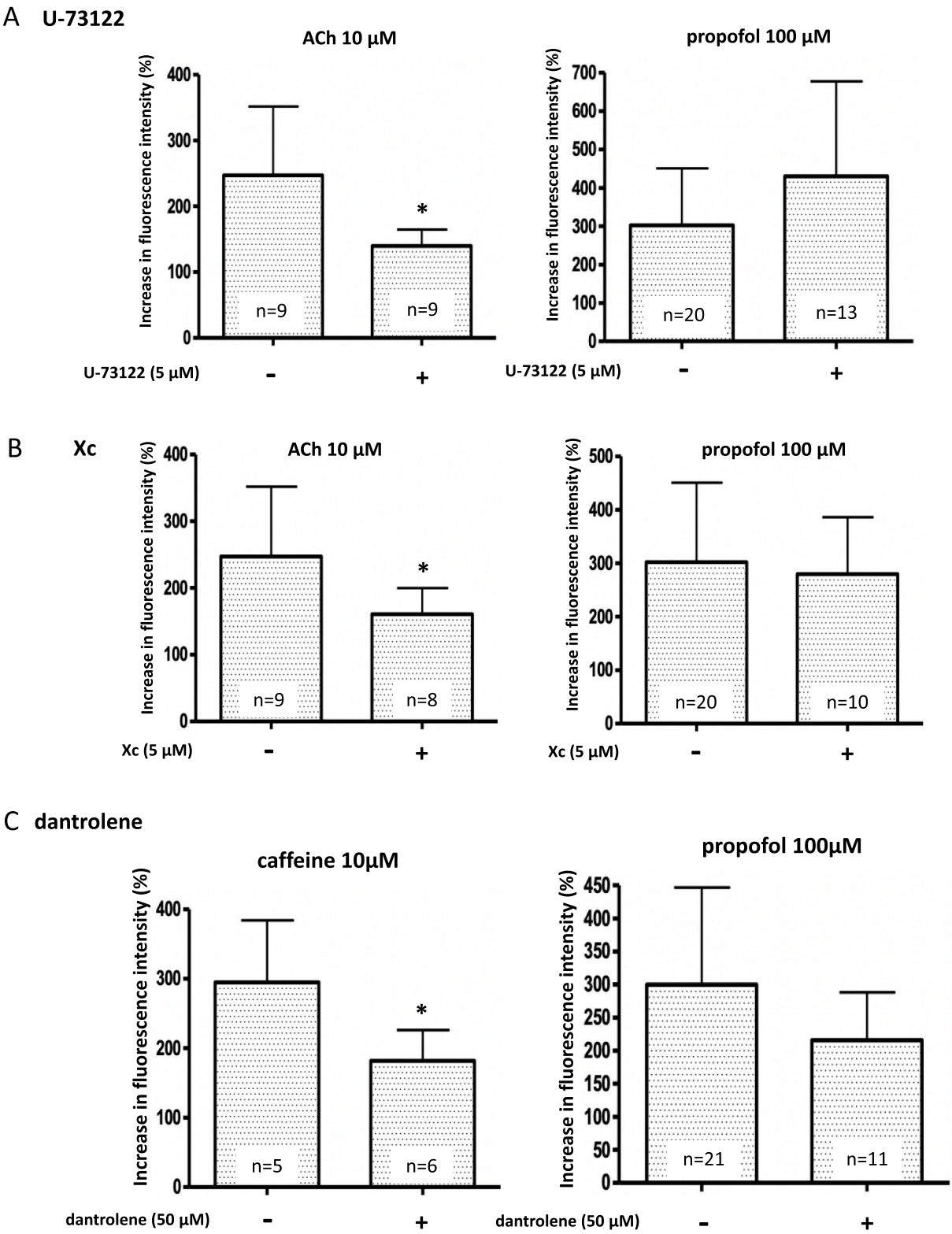

Fig. 3. Characterization of propofol-induced calcium elevation: The involvement of G-protein coupled receptors and IP_3 receptors.
(A) U-73122, a phospholipase C (PLC) inhibitor, at 5 μM significantly inhibited 10 μM acetylcholine-induced calcium elevation in SHSY-5Y cells (N = 7–9, *P < 0.05, compared to control, unpaired *t*-test). In contrast, U-73122 did not significantly affect propofol (100 μM)-induced calcium elevation. Data represent the mean ± SD (N = 13–21, P > 0.05, unpaired *t*-test). (B) Xestospongin C (Xc), an inositol 1,4,5-triphosphate receptor (IP_3R) antagonist, at 5 μM significantly inhibited 10 μM acetylcholine-induced calcium elevation in SHSY-5Y cells. Data represent the mean ± SD (N = 8–9, *P < 0.05, compared to control, unpaired *t*-test). In contrast, Xc at 5 μM did not significantly affect the propofol-induced calcium elevation Data represent the mean ± SD (N = 10–20, P > 0.05, compared to control, unpaired *t*-test). (C) Characterization of calcium elevation by propofol: The involvement of ryanodine receptors. Caffeine, a ryanodine receptor (RYR) agonist, at 10 μM induced intracellular calcium in SHSY-5Y cells. Dantrolene, a RYR antagonist, at 50 μM significantly inhibited caffeine-induced calcium mobilization. Data represent the mean ± SD (N = 5–6, *P < 0.05, compared to control, unpaired *t*-test); however, dantrolene at 50 μM did not significantly influence the propofol-induced calcium elevation (N = 11–21, P > 0.05, compared to control, unpaired *t*-test).

μM did not significantly affect the propofol-induced calcium elevation (Fig. 3B). These results suggest that the elevation of intracellular calcium by propofol might not be mediated by IP_3 receptors.

In addition, we also investigated the effects of dantrolene, a RyR antagonist, on propofol-induced calcium elevation. First, we examined the effects of dantrolene on calcium mobilization elicited by caffeine, a RyR agonist. The results demonstrated that dantrolene at 50 μM significantly inhibited 10 μM caffeine-induced calcium mobilization; however, dantrolene did not significantly influence propofol-induced calcium elevation (Fig. 3C), suggesting that propofol-induced calcium elevation might not be mediated via RyRs.

3.6. The influence of propofol on intracellular organelles

3.6.1. Observation of propofol-induced morphological changes in the ER by ER-Tracker™ RED

To further elucidate the mechanism underlying propofol-induced calcium elevation, we focused on the ER itself. ER-Tracker™ RED dye is a cell-permeant marker that is capable of staining the ER in living cells with high selectivity. ER-Tracker was loaded into cells before propofol application, and the ER status was observed during propofol stimulation.

In SHSY-5Y cells, propofol caused morphological changes in the ER that suggested fragmentation or aggregation within 5–7 min after the application of propofol (Fig. 4A, upper: a fluorescence microscopy image taken after 75 μM propofol application, lower: a confocal microscopy image taken after 100 μM propofol application, see Video, Supplemental Digital Content 2, which demonstrates 100 μM propofol-induced morphological changes of ER). In addition, we also observed propofol-induced morphological changes in the ER at each concentration between 0 and 200 μM by ER tracker. Propofol at concentrations greater than 50 μM induced apparent morphological changes in the ER in a dose-dependent manner (Supplemental Figs. 2A and 2B). Judging from the data by confocal laser scanning microscope, the morphological change of ER was sustainable during the observation period.

Supplementary video related to this article can be found at https://doi.org/10.1016/j.ejphar.2020.173303

3.6.2. Immunohistochemical confirmation of ER morphological changes

To further confirm propofol-induced morphological changes in the ER, propofol (100 μM)-treated COS-7 cells were immunohistochemically stained with an antibody against SEC61B, an ER marker, and visualized with an Alexa 488-conjugated secondary antibody. For immunohistochemical confirmation of ER morphological changes, we selected COS-7 cells because the ER structure of COS-7 cells is clearer and more developed than that of SHSY-5Y cells.

Three-dimensional imaging was performed using a confocal scanning microscope. The peripheral string-like structure of the ER was disrupted by propofol (Fig. 4B).

3.6.3. Observation of propofol-induced ER morphological changes using SERTΔCT-expressing COS-7 cells

The serotonin transporter (SERT) is functionally regulated via its membrane trafficking. Our previous study reported that the SERT C-terminal deletion mutant (SERTΔCT) show a robust decrease in its membrane trafficking and is mostly retained in the ER. This finding suggests that SERTΔCT is a beneficial marker protein of the ER for observing its precise structure (Asano et al., 2019). Therefore, we attempted to observe propofol-induced morphological changes in the ER in detail using SERTΔCT-expressing COS-7 cells. Two days after transfection, immunocytochemistry for FLAG-SERTΔCT-expressing COS-7 cells was carried out. Confocal microscopy images showed that the network formation of the peripheral ER was disrupted by propofol (Supplemental Fig. 5).

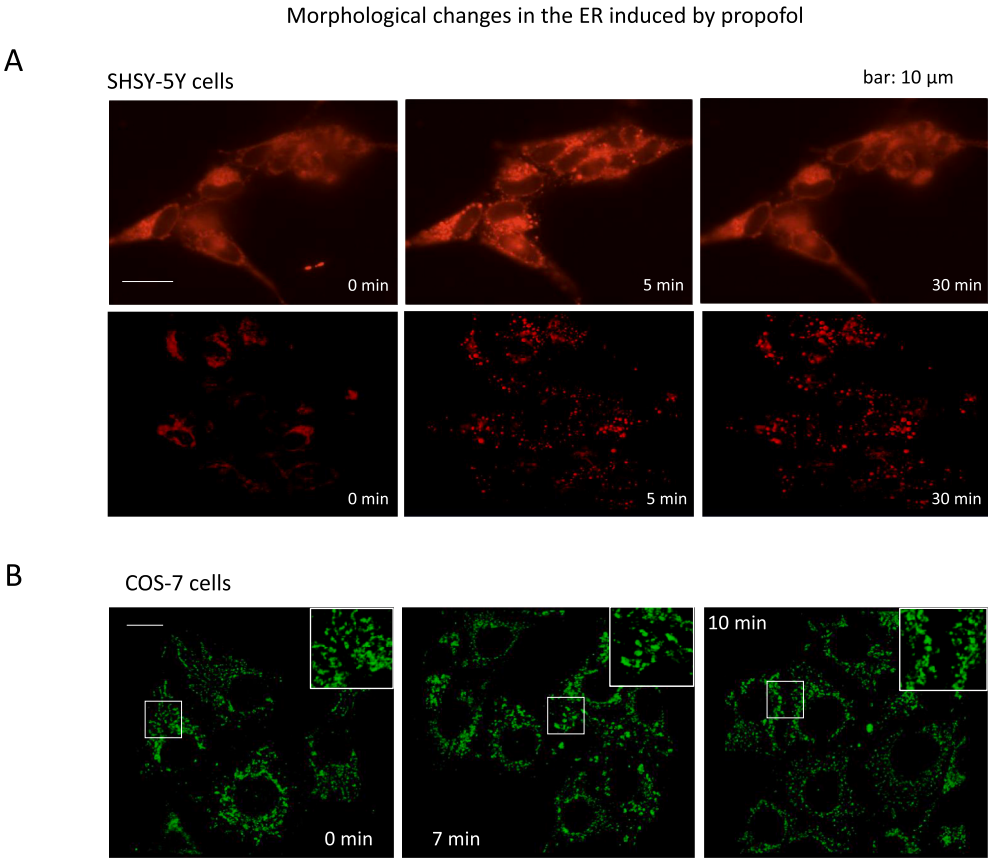

Fig. 4. Propofol-induced morphological changes in the ER.
(A) In the ER of SHSY-5Y cells, morphological changes such as fragmentation and aggregation were observed within 5–7 min after the application of propofol (upper: a fluorescence microscopy image taken after 75 μM propofol application; lower: a confocal microscopy image taken after 100 μM propofol application). (B) Immunohistochemical confirmation of ER morphological changes. Propofol (100 μM)-treated COS-7 cells were immunohistochemically stained with an antibody against SEC61B, an ER marker, and visualized with an Alexa 488-conjugated secondary antibody. Disruption of the peripheral string-like structure of the ER by propofol was observed by confocal scanning microscopy imaging. Insets represent the magnified images of indicated regions. The bars indicate 10 μm.

3.6.4. Influence of intracellular and extracellular calcium on morphological changes in the ER

To investigate the influences of intracellular and extracellular calcium on morphological changes in the ER, images of ER-tracker staining were observed when extracellular calcium was eliminated (Fig. 5A) or intracellular calcium was chelated by 50 μM BAPTA-AM (Fig. 5B). Fluorescence microscopy imaging showed that propofol (100 μM) caused morphological changes in the ER under both conditions.

In contrast to the finding that propofol-induced calcium elevation was abolished upon the removal of intracellular calcium, the morphological changes in the ER induced by propofol were revealed to be independent of intracellular calcium.

3.6.5. Temporal comparison of propofol-induced calcium elevation and morphological changes in the ER

Time-lapse imaging of the calcium indicator Fluo-4 (green) and ER-Tracker (red) was simultaneously carried out using a fluorescence microscope to determine whether calcium elevation or ER morphological changes occurred first. The calcium elevation was almost concurrent with morphological changes in the ER (Fig. 5C), indicating that both events occurred almost simultaneously. In addition, calcium elevation and morphological changes in the ER were observed in COS-7 cells, HEK293 cells and HUVECs exposed to propofol as well as SHSY-5Y cells (Supplemental Figs. 3 and 4).

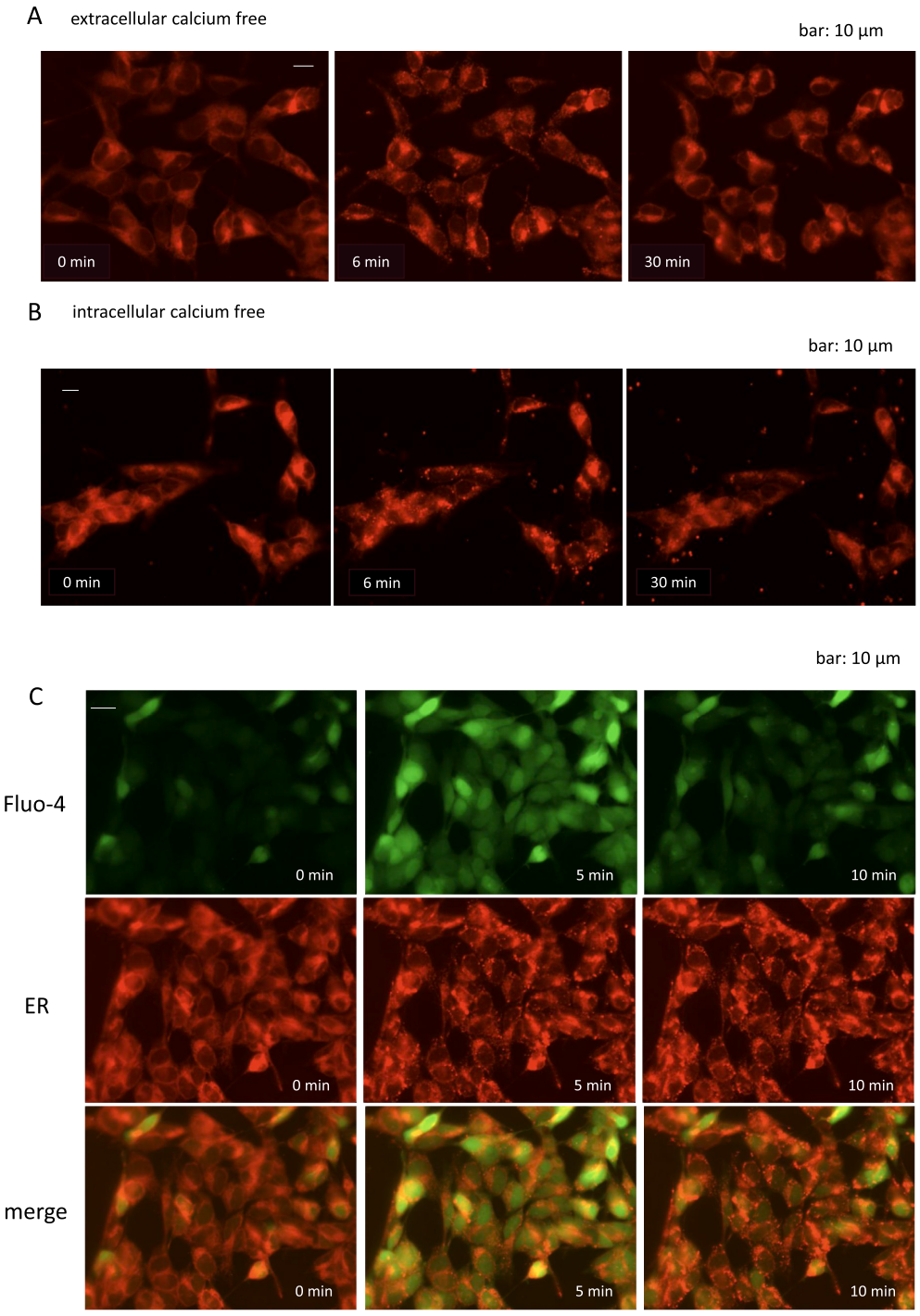

Fig. 5. Characterization of propofol-induced morphological changes in the ER.
(A) Fluorescence microscopy images of the ER loaded with ER-tracker after extracellular calcium was eliminated are shown. Treatment with 100 μM propofol caused morphological changes in the ER in the absence of extracellular calcium. (B) Fluorescence microscopy images of the ER loaded with ER-tracker when intracellular calcium was chelated by 50 μM BAPTA-AM are shown. Propofol (100 μM) caused morphological changes in the ER even in the absence of intracellular calcium. The bars indicate 10 μm. (C) Simultaneous time-lapse imaging of the calcium indicator Fluo-4 (Green) and ER-tracker (Red) was carried out using a fluorescence microscope. The calcium elevation was almost concurrent with the morphological changes in the ER. The actual time difference between when the green and red fluorescent signals were captured was appropriately 6 s. The bars indicate 10 μm.

3.6.6. Propofol-induced morphological changes in mitochondria

Mitochondria from living SHSY-5Y and COS-7 cells were stained with Mito Tracker™ ResCMXRos (250 nM), a red fluorescent dye that stains mitochondria in living cells, the accumulation of which is dependent on the membrane potential, using a similar method as that used for ER-tracker staining. Confocal microscopy images revealed that propofol (100 μM) induced morphological changes in mitochondria as well as the ER in both SHSY-5Y and COS-7 cells (Fig. 6). In contrast to ER and mitochondria, no prominent morphological change was not seen in Golgi apparatus (Supplemental Fig. 6).

3.7. Clinically used propofol also causes an elevation in intracellular calcium

In clinical use, propofol is dissolved in solvents, including lipid ingredients. We examined whether, like propofol alone, propofol that is clinically used causes intracellular calcium elevation. Clinically used 1% propofol was diluted to a concentration of 100 μM with ethanol and buffer to observe propofol-induced calcium elevation. Solvent alone without propofol was similarly diluted and used as the control. As shown in Supplemental Fig. 7 and 100 μM propofol prepared from 1% propofol elicited calcium elevation, while solvent alone did not.

3.8. 2,4-Diisopropylphenol-induced intracellular calcium elevation and morphological changes in the ER in SHSY-5Y cells

2,4-Diisopropylphenol is known as an isomer of propofol (Supplemental Fig. 8A). (Tsuchiya et al., 2010) We observed a 2,4-diisopropylphenol-induced elevation of intracellular calcium at concentrations between 0 and 200 μM in SHSY-5Y cells. Supplemental Fig. 8B shows that 2,4-diisopropylphenol at concentrations greater than 25 μM significantly induced the elevation of intracellular calcium in a dose-dependent manner, indicating that the threshold for calcium elevation is higher for 2,4-diisopropylphenol than propofol. Similarly, ER-Tracker was loaded into cells before 2,4-diisopropylphenol application. We confirmed that 2,4-diisopropylphenol at concentrations greater than 25 μM elicited similar morphological changes in the ER within 4 min after the application of 2,4-diisopropylphenol as those observed after propofol application (Supplemental Fig. 8C).

4. Discussion

In this experiment, we clarified that propofol at concentrations greater than 50 μM significantly induced the elevation of intracellular calcium in a dose-dependent manner. Although the propofol-induced elevation of intracellular calcium has been reported (Qiao et al., 2017; Subramanian and Meyer, 1997; Yang et al., 2019), the propofol concentration required to induce this calcium elevation seems to be lower than what was previously reported, the reason for which is unknown. In addition, we believe that the propofol-induced elevation of intracellular calcium is a universal phenomenon since it was observed in other cell lines in addition to SHSY-5Y cells. There was no significant difference in the ability of propofol to elicit calcium elevation among these cell types.

Next, we tried to elucidate how the propofol-induced elevation of intracellular calcium occurs. Since the elevation of intracellular calcium is not influenced by the removal of extracellular calcium, it is unlikely that the elevation is due to influx from the extracellular fluid. However, propofol has been reported to elicit calcium influx through voltage-dependent calcium channels (Lawton et al., 2012; Liu et al., 2019) or transient receptor potential (TRP) channels (Nishimoto et al., 2015), which is inconsistent with the present findings. SHSY-5Y cells may not express propofol-sensitive ion channels or receptors.

We found that the propofol-induced elevation of intracellular calcium was almost abolished after eliminating intracellular calcium with BAPTA-AM. Furthermore, the propofol-induced elevation of intracellular calcium was hardly observed even when calcium was depleted in the ER. Based on these two findings, we hypothesize that the propofol-induced elevation of intracellular calcium is primarily due to calcium mobilization from the ER.

Subsequently, we attempted to elucidate the mechanism of calcium mobilization from the ER. It is possible that the GPCR-IP_3 receptor pathway or RyRs, as the principal mechanisms of calcium mobilization from the ER, are involved. Therefore, we investigated the effects of an inhibitor of PLC (U-73122), an effector downstream of GPCRs, an IP_3R antagonist (Xc), and an RyR antagonist (dantrolene). However, they did not significantly influence propofol-induced calcium elevation. In a

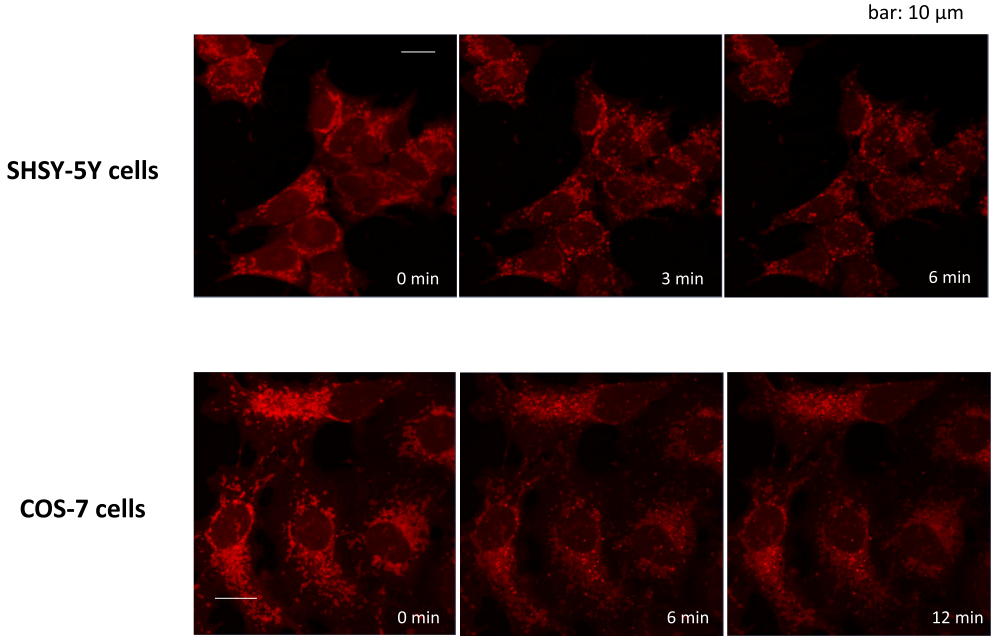

Fig. 6. Propofol-induced morphological changes in mitochondria.
Mitochondria from SHSY-5Y and COS-7 cells were stained with Mito Tracker™ ResCMXRos (250 nM), a red fluorescent dye. Confocal microscopy images demonstrated that 100 μM propofol induced morphological changes in mitochondria in both SHSY-5Y and COS-7 cells. The bars indicate 10 μm.

previous report, the propofol-induced elevation of calcium was suppressed by Xc or dantrolene (Yang et al., 2019), which differs from our present results for unknown reasons. As shown in Fig. 4, dantrolene tended to decrease the propofol-induced calcium elevation; however, it was not a significant change. Even if RyRs are involved in the mechanism of the propofol-induced calcium elevation, they seem to be a part of the mechanism. Further experiments are required to confirm these using cells other than SHSY-5Y cells.

Here, we focused on the ER itself to investigate the mechanism. As shown in Fig. 5, it seems that propofol changed the morphology of the ER, which appeared to be fragmented or aggregated. This finding was confirmed by immunohistochemical examinations of SEC61B and localized changes in SERTΔCT. In addition, propofol caused morphological changes not only in the ER but also in mitochondria. Since morphological changes in the ER were also observed in cells other than SHSY-5Y cells, this phenomenon appears to be universal regardless of cell type.

We investigated the relationship between morphological changes in the ER and propofol-induced calcium elevation. Morphological changes in the ER were observed even when no intracellular calcium elevation was observed after the elimination of intracellular calcium (Fig. 6). Also, intracellular calcium elevation and morphological changes in the ER occurred almost simultaneously. Considering that the cell membranes are permeable to propofol with high lipid solubility, the penetration of propofol was predicted to cause morphological changes by directly acting on the intracellular organelles that store calcium, resulting in the leakage of calcium into the cytosol. Since propofol also caused morphological changes in mitochondria, calcium mobilization from mitochondria may also be involved.

We demonstrated that 2,4-diisopropylphenol, an isomer of propofol, also caused intracellular calcium elevation and morphological changes in the ER, which is consistent with a previous report (Sumi et al., 2018). It is notable that the common structure of these reagents is related to the direct action of intracellular organelles on the membrane and their disruption of structure. We have considered a new possibility that propofol acts directly on intracellular organelles and causes calcium leakage by destroying the membrane structure, as a mechanism of intracellular calcium elevation. However, it is currently unknown why this highly lipophilic propofol or 2,4-diisopropylphenol destroys intracellular organelles such as the ER and mitochondria.

In this study, we found that the concentration of propofol that significantly induced an elevation of intracellular calcium and morphological changes in the ER was greater than 50 μM. Clinically, the blood concentration of propofol during general anesthesia is thought to be approximately 30 μM or less (Han et al., 2016; Kirkpatrick et al., 1988), therefore, the concentration used in the present study is apparently higher than that used clinically. However, it is possible that the concentration could reach greater than 30 μM at the site where propofol is injected into the blood vessel or in cases where propofol is used at a high dose. Therefore, the phenomena that we found in this study could be involved in the well-known incidence of propofol-induced angialgia. It is notable that this phenomenon was seen even in HUVECs, vascular endothelial cells (ECs), which are directly exposed to propofol. In terms of the mechanism underlying angialgia, the elevated calcium by propofol causes an increase in the phosphorylation of endothelial nitric oxide synthase (eNOS) at Ser^{1177} through calcium/calmodulin-dependent protein kinase II (CaM kinase II) or protein kinase C (PKC) isoforms in ECs (Fleming et al., 2001; Partovian et al., 2005; Wang et al., 2010). The enhancement of endothelial-derived NO production dilates the peripheral blood vessels at the injection site, causing the peripheral nerves surrounding ECs to stretch, which may trigger angialgia. We have already confirmed that various subtypes of PKC induced PKC translocation in SHSY-5Y cells and HUVECs, which may play an important role in the mechanism of propofol-induced eNOS activation and subsequent NO production. In our preliminary study, we have obtained the data showing the direct activation of PKCs at various subcellular regions in vivo (data not shown). Alternatively, it is possible that other unknown bioactive factors produced by propofol-induced calcium elevation might elicit surrounding sensory nerve terminals.

Regarding PRIS, accumulated propofol in cells possibly act on intracellular organelles including mitochondria and trigger morphological alternations. These predictions are supported by some studies showing that propofol acts directly on mitochondria (Felix et al., 2017; Wang et al., 2016). Additionally, PRIS has been noted to occur due to mitochondrial dysfunction (Finsterer and Frank, 2016; Vollmer et al., 2018), which is consistent with our study.

The elevation of intracellular calcium can activate various cellular signaling pathways, leading to the idea that the phenomena demonstrated in this study may be involved in the exertion of protective or toxic effects of propofol on cells. Further in vivo and human studies are necessary to elucidate the clinical significance of this study.

5. Conclusion

Our present data indicate that propofol induces a dose-dependent elevation of intracellular calcium in SHSY-5Y cells as well as COS-7 cells, HEK293 cells, and HUVECs. Accompanying the calcium elevation, the structure of the ER and mitochondria is fragmented and aggregated by unknown mechanism. These phenomena might be involved in the exertion of various adverse effects of propofol such as angialgia. Further experiments are required to elucidate the mechanism of propofol-induced calcium elevation and morphological changes in intracellular organelles.

Declaration of competing interest

The authors declare no conflict of interest regarding this study.

CRediT authorship contribution statement

Tomoaki Urabe: Conceptualization, Methodology, Formal analysis, Investigation, Writing - original draft. **Yuhki Yanase:** Resources. **Serika Motoike:** Resources. **Kana Harada:** Validation, Data curation. **Izumi Hide:** Validation, Data curation. **Shigeru Tanaka:** Validation, Data curation. **Yasuo M. Tsutsumi:** Supervision, Funding acquisition. **Masashi Kawamoto:** Supervision, Funding acquisition. **Norio Sakai:** Conceptualization, Methodology, Validation, Writing - review & editing, Supervision, Funding acquisition.

Acknowledgments

The author would like to thank Professor Yukihito Higashi (Department of Human Genetics, Research Institute for Radiation Biology and Medicine, Hiroshima University) for his scientific support and advice. Additionally, we appreciate Ms. Kasumi Terada (secretary of the Department of Anesthesiology and Critical Care, Hiroshima University) for her assistance. This work was performed using equipment at the Radiation Research Center for Frontier Science, Natural Science Center for Basic Research and Development, Hiroshima University and Biosignal Research Center, Kobe University.

Appendix A. Supplementary data

Supplementary data to this article can be found online at https://doi.org/10.1016/j.ejphar.2020.173303.

Funding statement

This study was supported by a Grant-in-Aid for Scientific Research from the Ministry of Education, Sports and Culture, Japan and by grants from the Takeda Science Foundation, Japan the Uehara Memorial Foundation, Japan and the Japanese Smoking Research Association.

References

Alkire, M.T., Hudetz, A.G., Tononi, G., 2008. Consciousness and anesthesia. Science 322, 876–880.

Asano, M., Motoike, S., Yokota, C., Usuki, N., Yamamoto, H., Urabe, T., Katarao, K., Hide, I., Tanaka, S., Kawamoto, M., Irifune, M., Sakai, N., 2019. SKF-10047, a prototype Sigma-1 receptor agonist, augmented the membrane trafficking and uptake activity of the serotonin transporter and its C-terminus-deleted mutant via a Sigma-1 receptor-independent mechanism. J. Pharmacol. Sci. 139, 29–36.

Cox, C.E., Reed, S.D., Govert, J.A., Rodgers, J.E., Campbell-Bright, S., Kress, J.P., Carson, S.S., 2008. Economic evaluation of propofol and lorazepam for critically ill patients undergoing mechanical ventilation. Crit. Care Med. 36, 706–714.

Felix, L.M., Correia, F., Pinto, P.A., Campos, S.P., Fernandes, T., Videira, R., Oliveira, M. M., Peixoto, F.P., Antunes, L.M., 2017. Propofol affinity to mitochondrial membranes does not alter mitochondrial function. Eur. J. Pharmacol. 803, 48–56.

Finsterer, J., Frank, M., 2016. Propofol is mitochondrion-toxic and may unmask a mitochondrial disorder. J. Child Neurol. 31, 1489–1494.

Fleming, I., Fisslthaler, B., Dimmeler, S., Kemp, B.E., Busse, R., 2001. Phosphorylation of Thr(495) regulates Ca(2+)/calmodulin-dependent endothelial nitric oxide synthase activity. Circ. Res. 88, E68–E75.

Franks, N.P., 2006. Molecular targets underlying general anaesthesia. Br. J. Pharmacol. 147 (Suppl. 1), S72–S81.

Gao, J., Peng, S., Xiang, S., Huang, J., Chen, P., 2014. Repeated exposure to propofol impairs spatial learning, inhibits LTP and reduces CaMKIIalpha in young rats. Neurosci. Lett. 560, 62–66.

Han, L., Fuqua, S., Li, Q., Zhu, L., Hao, X., Li, A., Gupta, S., Sandhu, R., Lonart, G., Sugita, S., 2016. Propofol-induced inhibition of catecholamine release is reversed by maintaining calcium influx. Anesthesiology 124, 878–884.

Hemphill, S., McMenamin, L., Bellamy, M.C., Hopkins, P.M., 2019. Propofol infusion syndrome: a structured literature review and analysis of published case reports. Br. J. Anaesth. 122, 448–459.

Irifune, M., Takarada, T., Shimizu, Y., Endo, C., Katayama, S., Dohi, T., Kawahara, M., 2003. Propofol-induced anesthesia in mice is mediated by gamma-aminobutyric acid-A and excitatory amino acid receptors. Anesth. Analg. 97, 424–429 table of contents.

Kirkpatrick, T., Cockshott, I.D., Douglas, E.J., Nimmo, W.S., 1988. Pharmacokinetics of propofol (diprivan) in elderly patients. Br. J. Anaesth. 60, 146–150.

Kotani, Y., Shimazawa, M., Yoshimura, S., Iwama, T., Hara, H., 2008. The experimental and clinical pharmacology of propofol, an anesthetic agent with neuroprotective properties. CNS Neurosci. Ther. 14, 95–106.

Lawton, B.K., Brown, N.J., Reilly, C.S., Brookes, Z.L., 2012. Role of L-type calcium channels in altered microvascular responses to propofol in hypertension. Br. J. Anaesth. 108, 929–935.

Li, X., Yao, L., Liang, Q., Qu, H., Cai, H., 2018. Propofol protects hippocampal neurons from hypoxia-reoxygenation injury by decreasing calcineurin-induced calcium overload and activating YAP signaling. Oxid. Med. Cell. Longevity 2018, 1725191.

Liang, W.Z., Jan, C.R., Lu, C.H., 2012. Investigation of 2,6-diisopropylphenol (propofol)-evoked Ca2+ movement and cell death in human glioblastoma cells. Toxicol. Vitro : an international journal published in association with BIBRA 26, 862–871.

Liu, Q.Z., Hao, M., Zhou, Z.Y., Ge, J.L., Wu, Y.C., Zhao, L.L., Wu, X., Feng, Y., Gao, H., Li, S., Xue, L., 2019. Propofol reduces synaptic strength by inhibiting sodium and calcium channels at nerve terminals. Protein Cell 10, 688–693.

Liu, X.R., Cao, L., Li, T., Chen, L.L., Yu, Y.Y., Huang, W.J., Liu, L., Tan, X.Q., 2017. Propofol attenuates H2O2-induced oxidative stress and apoptosis via the mitochondria- and ER-medicated pathways in neonatal rat cardiomyocytes. Apoptosis : Int. J. Program. Cell Death 22, 639–646.

Miyahara, T., Adachi, N., Seki, T., Hide, I., Tanaka, S., Saito, N., Irifune, M., Sakai, N., 2018. Propofol induced diverse and subtype-specific translocation of PKC families. J. Pharmacol. Sci. 137, 20–29.

Nakajima, A., Tsuji, M., Inagaki, M., Tamura, Y., Kato, M., Niiya, A., Usui, Y., Oguchi, K., 2014. Neuroprotective effects of propofol on ER stress-mediated apoptosis in neuroblastoma SH-SY5Y cells. Eur. J. Pharmacol. 725, 47–54.

Nishimoto, R., Kashio, M., Tominaga, M., 2015. Propofol-induced pain sensation involves multiple mechanisms in sensory neurons. Pflueg. Arch. Eur. J. Physiol. 467, 2011–2020.

Nobukuni, M., Mochizuki, H., Okada, S., Kameyama, N., Tanaka, A., Yamamoto, H., Amano, T., Seki, T., Sakai, N., 2009. The C-terminal region of serotonin transporter is important for its trafficking and glycosylation. J. Pharmacol. Sci. 111, 392–404.

Partovian, C., Zhuang, Z., Moodie, K., Lin, M., Ouchi, N., Sessa, W.C., Walsh, K., Simons, M., 2005. PKCalpha activates eNOS and increases arterial blood flow in vivo. Circ. Res. 97, 482–487.

Qiao, H., Li, Y., Xu, Z., Li, W., Fu, Z., Wang, Y., King, A., Wei, H., 2017. Propofol affects neurodegeneration and neurogenesis by regulation of autophagy via effects on intracellular calcium homeostasis. Anesthesiology 127, 490–501.

Subramanian, K., Meyer, T., 1997. Calcium-induced restructuring of nuclear envelope and endoplasmic reticulum calcium stores. Cell 89, 963–971.

Sumi, C., Okamoto, A., Tanaka, H., Nishi, K., Kusunoki, M., Shoji, T., Uba, T., Matsuo, Y., Adachi, T., Hayashi, J.I., Takenaga, K., Hirota, K., 2018. Propofol induces a metabolic switch to glycolysis and cell death in a mitochondrial electron transport chain-dependent manner. PloS One 13, e0192796.

Sun, B., Ou, H., Ren, F., Huan, Y., Zhong, T., Gao, M., Cai, H., 2018. Propofol inhibited autophagy through Ca(2+)/CaMKKbeta/AMPK/mTOR pathway in OGD/R-induced neuron injury. Mol. Med. 24, 58.

Tsuchiya, H., Ueno, T., Tanaka, T., Matsuura, N., Mizogami, M., 2010. Comparative study on determination of antioxidant and membrane activities of propofol and its related compounds. Eur. J. Pharmaceut. Sci. : Off. J. Eur. Fed. Pharmaceut. Sci. 39, 97–102.

Vasile, B., Rasulo, F., Candiani, A., Latronico, N., 2003. The pathophysiology of propofol infusion syndrome: a simple name for a complex syndrome. Intensive Care Med. 29, 1417–1425.

Velly, L.J., Guillet, B.A., Masmejean, F.M., Nieoullon, A.L., Bruder, N.J., Gouin, F.M., Pisano, P.M., 2003. Neuroprotective effects of propofol in a model of ischemic cortical cell cultures: role of glutamate and its transporters. Anesthesiology 99, 368–375.

Vollmer, J.P., Haen, S., Wolburg, H., Lehmann, R., Steiner, J., Reddersen, S., Fend, F., Fallier-Becker, P., 2018. Propofol related infusion syndrome: ultrastructural evidence for a mitochondrial disorder. Crit. Care Med. 46, e91–e94.

Wang, H., Zheng, S., Liu, M., Jia, C., Wang, S., Wang, X., Xue, S., Guo, Y., 2016. The effect of propofol on mitochondrial fission during oxygen-glucose deprivation and reperfusion injury in rat hippocampal neurons. PloS One 11, e0165052.

Wang, L., Wu, B., Sun, Y., Xu, T., Zhang, X., Zhou, M., Jiang, W., 2010. Translocation of protein kinase C isoforms is involved in propofol-induced endothelial nitric oxide synthase activation. Br. J. Anaesth. 104, 606–612.

Yang, M., Wang, Y., Liang, G., Xu, Z., Chu, C.T., Wei, H., 2019. Alzheimer's disease presenilin-1 mutation sensitizes neurons to impaired autophagy flux and propofol neurotoxicity: role of calcium dysregulation. J. Alzheim. Dis. : JAD 67, 137–147.

Zhou, X., Wei, Y., Qiu, S., Xu, Y., Zhang, T., Zhang, S., 2016. Propofol decreases endoplasmic reticulum stress-mediated apoptosis in retinal pigment epithelial cells. PloS One 11, e0157590.